EFDA–JET–PR(11)39

F. Belli, S. Conroy, B. Esposito, L. Giacomelli, V. Kiptily, A. Lücke, D. Marocco,
M. Riva, H. Schuhmacher, B. Syme, K. Tittelmeier, A. Zimbal
and JET EFDA contributors

Conceptual Design, Development and Preliminary Tests of a Compact Neutron Spectrometer for the JET Experiment

“This document is intended for publication in the open literature. It is made available on the understanding that it may not be further circulated and extracts or references may not be published prior to publication of the original when applicable, or without the consent of the Publications Officer, EFDA, Culham Science Centre, Abingdon, Oxon, OX14 3DB, UK.”

“Enquiries about Copyright and reproduction should be addressed to the Publications Officer, EFDA, Culham Science Centre, Abingdon, Oxon, OX14 3DB, UK.”

The contents of this preprint and all other JET EFDA Preprints and Conference Papers are available to view online free at www.iop.org/Jet. This site has full search facilities and e-mail alert options. The diagrams contained within the PDFs on this site are hyperlinked from the year 1996 onwards.

Conceptual Design, Development and Preliminary Tests of a Compact Neutron Spectrometer for the JET Experiment

F. Belli[1], S. Conroy[2,7], B. Esposito[1], L. Giacomelli[3,7], V. Kiptily[4], A. Lücke[5], D. Marocco[1], M. Riva[1], H. Schuhmacher[5], B. Syme[4], K. Tittelmeier[5], A. Zimbal[5] and JET EFDA contributors*

JET-EFDA, Culham Science Centre, OX14 3DB, Abingdon, UK

[1]Associazione EURATOM-ENEA sulla Fusione, C.R. Frascati, C.P. 65, Frascati I-00044, Roma, Italy.
[2]Department of Physics and Astronomy, Uppsala University, BOX 516, SE-75120 Uppsala, Sweden.
[3]Dipartimento di Fisica, Università degli Studi di Milano-Bicocca, and Istituto di Fisica del Plasma,
Associazione EURATOM-ENEA-CNR, 20100 Milano, Italy.
[4]EURATOM-CCFE Fusion Association, Culham Science Centre, OX14 3DB, Abingdon, OXON, UK
[5]Physikalisch-Technische Bundesanstalt, Bundesallee 100, 38116 Braunschweig, Germany.
[6]Association EURATOM-UKAEA/JOC, Culham Science Centre, Abingdon, UK.
[7]JET-EFDA, Culham Science Centre, OX14 3DB, Abingdon, UK.
** See annex of F. Romanelli et al, "Overview of JET Results",*

Preprint of Paper to be submitted for publication in
IEEE Transactions on Nuclear Science

ABSTRACT

A Compact Neutron Spectrometer (CNS) has been developed to measure the neutron emission spectra in Joint European Torus (JET) fusion plasma experiments. The spectrometer, based on a liquid scintillation detector (BC501A), is equipped with a Digital Pulse Shape Discrimination (DPSD) acquisition system for neutron (n) and gamma-ray (γ) separation. The CNS enables recording the n and γ Pulse Height Spectra (PHS) up to total count rates of ~ 10^6 s^{-1}. Energy resolution, after PHS unfolding, will be < 2% for 14MeV neutrons and < 4% for 2.5MeV neutrons. The work done by ENEA-Frascati and Physikalisch-Technische Bundesanstalt (PTB) respectively in the assembly and test of DPSD and scintillation detector, along with the first results obtained by the spectrometer in JET plasma experiments are presented. The experience obtained with CNS in JET will contribute to the development of neutron spectrometers suitable for applications in the International Thermonuclear Experimental Reactor (ITER).

1. INTRODUCTION

The JET Compact Neutron Spectrometer (CNS) is designed to measure the neutron emission spectrum in different plasmas scenarios. The spectrometer views the horizontal port of Octant 7 at an angle of 22.5° to the normal (see Fig.1). The line of sight lies in a horizontal plane 135mm above the midplane of the machine (i.e., typically 165mm below the center of the plasma), and has a significant component tangential to the toroidal field lines [1].

The main components of the instrument are a liquid scintillation detector (BC501A) for n and γ detection, coupled to a Photomultiplier (PMT) connected to a Digital Pulse Shape Discrimination (DPSD) acquisition system [2]. The CNS enables the recording of separate n and γ pulse height spectra at total count rates up to ~ 10^6 s^{-1}. After unfolding the neutron spectra can be determined with energy resolution < 2% at 14MeV and < 4% at 2.5MeV [3].

We present here the design and performance tests of the DPSD and scintillation detector, along with the preliminary results of the assembled spectrometer during JET C27 experimental campaign. It is expected that the operation of CNS in JET campaigns will contribute to the development of neutron spectrometers suitable for applications in ITER.

2. DPSD SYSTEM

2.1. SYSTEM ARCHITECTURE

The DPSD system, model ENEA FUS-ING 07-011, comprises two 14-bit 100MSamples/s Analog to Digital Converters (ADCs), coupled in interleaved mode in order to obtain an actual sampling rate of 200MSamples/s on one input channel, a Field Programmable Gate Array (FPGA) and a high speed PCI board (maximum throughput 80MB/s) [4].

The 200 MSamples/s data stream is managed by a series of processing blocks programmed inside the FPGA: Dynamic Window Data Acquisition (DWDA, see below), Data Packing and Real-Time Processing (to be used for real-time control or testing purposes).

For detector characterization, to be performed by Time-of-Flight (T-o-F) measurements, the board has been supplied with an output connector providing a 10ns TTL pulse, 500ns after the triggering of incoming pulses.

2.2. DWDA

The DWDA block (see diagram in Fig.2) allows to sample data only when pulses are present, reducing in such a way the amount of stored data and increasing the maximum count rate sustainable by the system [2]. At first, an offset removal is performed on the stream of incoming data and, subsequently, over threshold pulses are selected. An endless acquisition ring is continuously filled by data: as soon as the threshold is reached, the data relative to the pulse (data acquisition window) is extracted and sent to the next block. If during the pre-programmed acquisition window another pulse arrives, the window length is increased to acquire the new incoming pulse. Such data acquisition window is sent to the Time/Data packing block, which packs it with the timing information of the first over threshold pulse sample. The data is then sent to the digital acquisition board to be acquired by the PC.

A maximum sustained count rate of ~ 900kHz has been reached in laboratory tests using a pulse generator producing pulses with average length of 32 samples (160ns). As every sample contains 2 Bytes and the pulse time stamp header has 6Bytes, each pulse results in 70Bytes, so that 900kHz means a sustained throughput of 63MB/s, close to the maximum PCI board throughput of 80MB/s.

2.3. PROCESSING SOFTWARE

The data acquisition from the PCI board and the storage into the PC RAM is handled by a real-time acquisition software written in C++ and integrated in a LabVIEW^{TM} executable module, used also for local off-line processing.

The processing software (see Fig.3) performs pile-up rejection and LED signal evaluation for PMT gain variation correction (see Section III) and provides separate n and γ Pulse Height Spectra (PHS) and count rates, allowing post experiment data reprocessing [5]. n/γ discrimination is obtained by means of the charge comparison method [6] while the energy of the particle is determined from the pulse charge integral (Q_T).

2.4. CHARACTERIZATION OF THE ADC ACQUISITION CHANNELS

The use of the interleaved technique can deteriorate the spectral purity of the reconstructed signal. In order to correct for this effect a calibration program running on the FPGA is used to acquire a sinusoidal signal (top panel of Fig.4) and determine from it a set of correction coefficients [2]. The mid and bottom panels of the figure show, respectively, the Fast Fourier Transforms (FFT) of uncorrected and corrected interleaved signal (left), with a zoom of the low frequency part of the spectra (right).

The uncorrected signal (mid panels of the figure) shows two unwanted features:

a) a DC component at zero frequency, due to the different offsets of the two channels;

b) a component at the sampling frequency, due to the different amplification factors.

In the bottom panels the results after the correction are shown: only the real signal survives, while the unwanted frequency components are reduced to intensity values below −80dB level.

3. DETECTOR

The CNS detector is based on the liquid organic scintillator BC501A, (25mm diameter × 25mm height) coupled to a Photonis XP2020 PMT through a light guide with an embedded Light Emitting Diode (LED) (1kHz frequency). The LED signal is used to correct for the PMT gain variations produced by variations of the incoming count rate [3] which would yield distorted PHS. An example of the PMT gain variation effect is shown in Fig. 5, where the results of a measurement performed irradiating a detection system similar to the CNS with the modulated 14MeV neutron beam produced by the PTB accelerator are presented [7]: a clear shift in the position of the LED in the PHS (right axis) that strictly follows the variations on the incoming count rate (left axis) is visible.

The BC501A scintillator implemented in the CNS allows neutron measurements in the energy range from 1.5 to 20MeV, i.e. of the 2.5MeV (DD) and 14MeV (DT) neutrons, and simultaneous recording of n and γ ray PHS.

3.1. TEMPERATURE STABILITY OF THE LED REFERENCE SIGNAL

The light emission of the LED and of the scintillating detector are both sensitive to temperature changes, and need to be compensated using a temperature sensor and a regulating circuit on the LED board. The pulsed light of the LED is amplified by the photomultiplier in the same way as signals from the scintillator.

In case of temperature changes, the LED signal can still be used to correct for the PMT gain variations produced by variations of the incoming count rate if the ratio of the pulse heights of pulses from a radioactive source (e.g. ^{22}Na) and LED pulses is constant for different temperatures [8]. A trimmer of the temperature control loop is adjusted until this constant ratio is obtained (maximum drift <0.5% for temperature range from 15°C to 35°C): in this case the measured difference between the PHS channel numbers of the two ^{22}Na edges for different temperatures is constant with temperature, as shown in Fig.6. This adjustment effectively means that the LED temperature dependence is adjusted to be the same as that of the light emission of the scintillator.

3.2. HOMOGENEITY OF THE PMT PHOTOCATHODE RESPONSE

A collimated ^{22}Na source has been used to selectively irradiate the detector at 10 different (5 radial and 5 axial) positions and the associated PHS were analyzed to determine the relative changes in the position of the 511keV Compton edge. The position of this Compton edge is a measure for the relative light yield (i.e., light collection efficiency) for irradiations of the detector at different incident positions on the PMT photocathode. The results obtained (see Fig.7) demonstrate a high homogeneity (within 2%) of the PMT photocathode response.

3.3. PULSE HEIGHT RESOLUTION

The pulse height resolution of the detector is checked with a ^{207}Bi γ source (three Compton edges for γ-lines of 570keV, 1063keV and 1770keV). The recorded PHS (see Fig.8) is analyzed by fitting each of the three Compton recoil edges (called peak1 to peak3 in the figure) with a combination of three Gaussian functions, obtaining the parameter mean values and FWHM needed to calculate the equivalent Gaussian resolution of the distribution. Note that the Q_T axis scale in Fig.8 is different from the ones in all the subsequent PHS figures, as it has been obtained with different analysis settings, optimized for the CNS calibration.

The resolution for the Compton edges obtained with the CNS DPSD board is 29.3%, 18.9% and 13.8% respectively.

4. PRELIMINARY RESULTS ON JET

JET C27 experimental campaign (July - October 2009) with Deuterium plasma has been a useful test bench for the assembled CNS, although the detector response function has not been determined yet. This means that unfolded neutron energy spectra cannot be produced: preliminary results are based on the discriminated n and γ PHS from JET plasma discharges. The γ PHS are the result of a ^{207}Bi calibration source and background emissions.

4.1. DETECTOR STABILITY

The first checks on CNS concerned the detector stability, through the monitoring of the positions of the ^{207}Bi Compton edges + LED peak, at PTB and JET, before and after installation into the bunker in which the detector has the line of sight depicted in Fig.1, giving variations of the positions of the Compton edges within 6% and of the LED peak within 3%, as shown in Fig.9. These variations are mainly due to the PMT stabilization and to different measurement conditions, i.e. cabling and LED temperature. For a fixed experimental setup, the system shows a much more stable behaviour. After applying the LED correction, the pulse height scale derived from the positions of the three Compton edges is constant within ±1-2% for measuring periods of a couple of weeks.

4.2. N AND γ DISCRIMINATION CAPABILITY

Discrimination between n and γ pulses can be difficult for low-energy pulses: the fraction of erroneously n/γ discriminated events as a function of their energy has been quantified by means of ^{207}Bi γ acquisitions (Fig.10). With optimized separation settings the fake neutron component is at maximum ~13% for Q_T = 5a.u. and rapidly decreases to 0.02% level for Q_T > 20 a.u., i.e., for neutron equivalent energies >1.6MeV. For data analysis, the Q_T = 8 a.u. threshold (above which the overall fake neutron contribution is less than 1%) has been used, as this is the maximum total integral value below which collected pulses can be discarded (via hardware or software threshold settings) without compromising neither the calibration measures (i.e. allowing a good fit of the first ^{207}Bi Compton edge) nor the neutron PHS unfolding. A maximum error of 1% on the neutron count

rates is then to be considered in all the following results. Fig 11 shows the n/γ separation plot for a JET plasma discharge using the optimized separation settings (horizontal segmented line) and Q_T = 8 a.u. threshold (vertical line).

4.3. N MEASUREMENTS

The JET D-D plasma generates both 2.5MeV and 14MeV neutrons. The 14MeV neutrons are the result of the triton burn-up process [9] in which 1.01MeV tritons originating from the D(d,p)T reaction (same branching ratio as the D(d,n)^{3}He reaction producing the 2.5MeV neutrons) react with D ions (D(t,n)^{4}He reaction) during their slowing down and produce neutrons with energies ≥14MeV. The tritons most likely do not thermalize but react before thermalization with bulk deuterons at energies >100 keV. Figure 12 shows an example (calculated using TRAP-T code [10], see below) of the energy spectrum for both 2.5MeV and 14MeV neutrons produced in a D-D plasma at JET with a typical value of the bulk temperature of 8keV: the ratio between 14MeV and 2.5MeV neutrons is 1.5 %.

Figure 13 shows n and γ PHS obtained from JET pulses with high Neutral Beam Injection (NBI) power (Pulse No: 78713, I_p = 3.8MA, B_t = 3.07T , P_{NBI} = 22MW, left) and low NBI power (Pulse No: 78807, I_p = 1.8MA, B_t = 3.3T, P_{NBI} = 1.3MW, right); the corresponding count rates measured by the CNS and the JET Fission Chamber (FC) neutron monitors show in Fig.14 the effect of the evolution of NBI power during the pulses.

The ratio of the total neutron yield measured by neutron monitors to the neutrons measured by the CNS (integral of counts in the spectrum) is different in the two cases: the CNS measured 7.12×10^5 neutrons in Pulse No: 78713, corresponding to an efficiency of 8.35×10^{-12} detected neutrons per JET produced neutron (neutrons/source neutron), and 6.09×10^4 neutrons in pulse no. 78807 corresponding to 1.37×10^{-11} neutrons/source neutron. This discrepancy of ~1.6 is related to neutron emission profile effect differences in the two discharges.

Figure 15 demonstrates the CNS capability of measuring simultaneously 2.5MeV and 14MeV neutrons in high power discharges (Pulse No: 78713). The 2.5MeV neutrons pulses measured with the CNS result in the continuous neutron spectrum up to about Q_T = 35 a.u. while 14MeV neutrons produce the higher pulses up to Q_T = 350 a.u..

The code TRAP-T at JET has been used to determine the triton burn-up emission to be compared with the experimental observations [10]. The code assumes a standard (i.e., not elongated) plasma shape and uses the plasma current I_p and the impurity level Z_{eff} as input parameters to calculate the 14MeV neutron emission from the tritons slowing down in the D plasmas. The losses due to the orbits of the fast tritons are not accounted for. TRAP-T calculations result in a 14 MeV neutron emission of (1.53 ± 0.30) % for Pulse No: 78713 and (1.45 ± 0.30) % for the low power Pulse No: 78807 (the errors quoted in the results are mainly due to Z_{eff} value uncertainties). For comparison with experimental data, an estimate of the triton burn-up 14MeV neutron emission is possible from the measured PHS, in which pulses in the range Q_T = [12, 100] a.u. can be associated to 2.5MeV neutrons and pulses in the range Q_T = [100, 450] to 14MeV neutrons. The contribution of

14MeV neutrons to the 2.5MeV range Q_T = [12, 100] a.u. is in this case negligible (less than 1 %). Moreover, the different detector efficiencies for 2.5MeV and 14MeV neutrons respectively in the selected energy ranges (the first is about 3 times the second) are taken into account. The estimates of the triton burn-up 14MeV neutron emission result (1.85 ± 0.03) % for Pulse No: 78713 and (0.96 ± 0.07) % for Pulse No: 78807 (statistical errors are quoted: the total relative errors, taking into account the detector efficiency uncertainties, are in the order of 10-15%). The measured and calculated triton burn-up values are comparable (within the errors) for Pulse No: 78713. On the contrary, a discrepancy is found for the second pulse: this might be due to parameters (e.g. plasma elongation) not taken in account in the present version of TRAP-T.

4.4. HARD X RAY MEASUREMENTS

Plasma disruptions and runaway electrons were studied in the JET experiments. Plasma disruptions generate highly accelerated electrons (runaways) [11], which produce Bremsstrahlung radiation in Coulomb collisions with plasma nuclei and the tokamak plasma facing materials. As previous results at JET have shown, the runaway energies range from few MeV [12] to several tens of MeV [13]. When the runaway energy is above the photoneutron emission reaction threshold, neutrons are also produced. Gamma and neutrons were detected both by JET Hard X-ray (HXR) and FC monitors and by the CNS spectrometer: the results for Pulse No: 78866, in which the disruption occurred at t = 24s, are shown in Fig.16. The top panel presents the plasma current (I_P), the bottom panel compares the corresponding evolutions of the gamma and neutron signals recorded by JET and CNS systems. The comparison demonstrates the good sensitivity of the CNS to both neutron and gamma and the agreement between the two detector systems.

Figure 17 shows the CNS PHS obtained in the time interval of Fig.16. The LED is pulsed at 1kHz and the radiation pulse shapes are corrected within 10 ms to account for PMT gain drift**.** The analysis of such PHS data can permit to study the evolution of the energy distribution of runaways during disruptions.

CONCLUSIONS

The design of the CNS, its testing procedures during the assembling phases and the first results obtained in JET experiments have been presented. Besides the stability of its components, its performances in different plasma scenarios have been tested, showing the CNS good capabilities of discriminating and recording the n and γ radiation produced during JET plasma discharges, in agreement with theoretical models and different monitoring instruments.

In the forthcoming JET experiments, after the detector characterization (i.e. after the determination of the relation between neutron energies and detector PHS), the unfolding of the recorded PHS will be performed. The determined neutron fluxes and energy spectra will allow a deeper analysis of plasma discharges.

ACKNOWLEDGMENTS

This work was supported by EURATOM and carried out within the framework of the European Fusion Development Agreement. The views and opinions expressed herein do not necessarily reflect those of the European Commission. This work has been partly funded by EFDA Contract FU06-CT-2006-00076 and EFDA-JET Task JW6-OEP-ENEA-58 (Compact Neutron Spectrometer).

REFERENCES

[1]. N.P. Hawkes, P. van Belle, D.S. Bond, S. Croft, and O.N. Jarvis, "A 14MeV neutron spectrometer for the Joint European Torus deuterium-tritium experiments", *Review of Scientific Instruments*, vol. **70**, no. 1, January 1999, pp 1134-1136.

[2]. M. Riva, B. Esposito, and D. Marocco, "A new pulse-oriented digital acquisition system for nuclear detectors", *Fusion Engineering and Design*, vol. **82**, issues 5-14, October 2007, pp 1245-1250.

[3]. A. Zimbal *et al*., "Compact NE213 neutron spectrometer with high energy resolution for fusion applications", *Review of Scientific Instruments*, vol. **75**, no. 10, October 2004, pp 3553-3555.

[4]. B. Esposito, M. Riva, D. Marocco and Y. Kaschuck, "A digital acquisition and elaboration system for nuclear fast pulse detection", *Nuclear Instruments and Methods in Physics Research A* **572** (2007) 355–357.

[5]. D. Marocco, M. Riva, B. Esposito, L. Bertalot, and A. Zimbal, "A digital data acquisition system optimized for spectrometry with liquid scintillation detectors", *Proceedings of Science*, FNDA2006, 028, 2006.

[6]. Knoll G. F., "Radiation detection and measurements", *John Wiley & Sons*, 2000.

[7]. D. Marocco *et al*., "High count rate neutron spectrometry with liquid scintillation detectors", *IEEE Transactions on Nuclear Science*, vol. **56**, no. 3, June 2009, pp 1168-1173.

[8]. K. Tittelmeier, H.-J. Barrenscheen, "Stabilisierung von Szintillationsdetektoren", *Laboratory Report PTB* 6.42-03-2, 2003.

[9]. G. Gorini, L. Ballabio and J. Källne, "Neutron spectrometry diagnostic of triton burn-up in deuterium fusion plasmas", *Plasma Physics and. Controlled Fusion* **39** (1997), pp 61-71.

[10]. S. Conroy, O. N. Jarvis, G. Sadler and G. B. Huxtable, "Time resolved measurements of triton burnup in JET plasmas", *Nuclear Fusion* **28** (1988) p. 2127.

[11]. V. Riccardo *et al*., "Disruption and disruption mitigation", Plasma Physics and Controlled Fusion **45** (2003) A269.

[12]. B. Esposito et al., "Runaway electron measurements in the JET tokamak", *Plasma Physics and Controlled Fusion* **38** (1996) 2035.

[13]. O.N. Jarvis et al., "Photoneutron production accompanying plasma disruptions in JET", *Nuclear Fusion* **28** (1988) 1981.

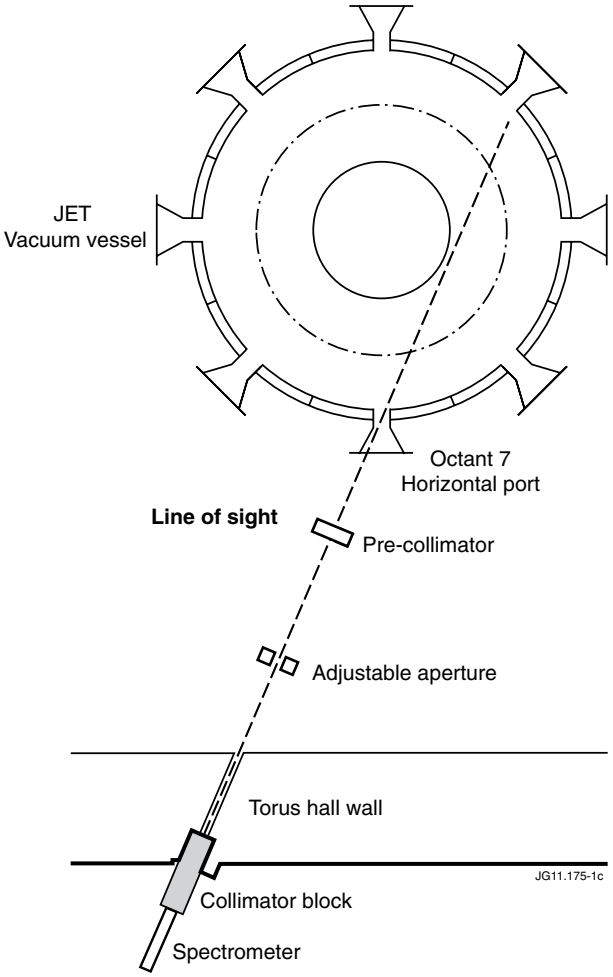

Figure 1: Line of sight of the CNS as installed at JET (from [1]).DPSD SYSTEM.

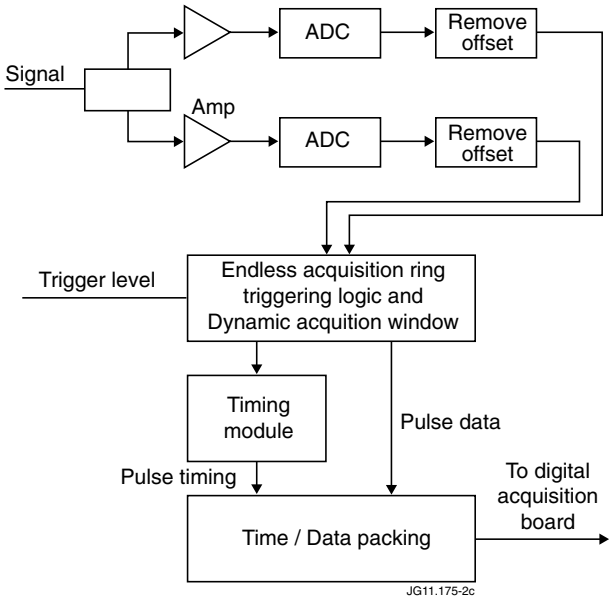

Figure 2: Dynamic Window Data Acquisition.

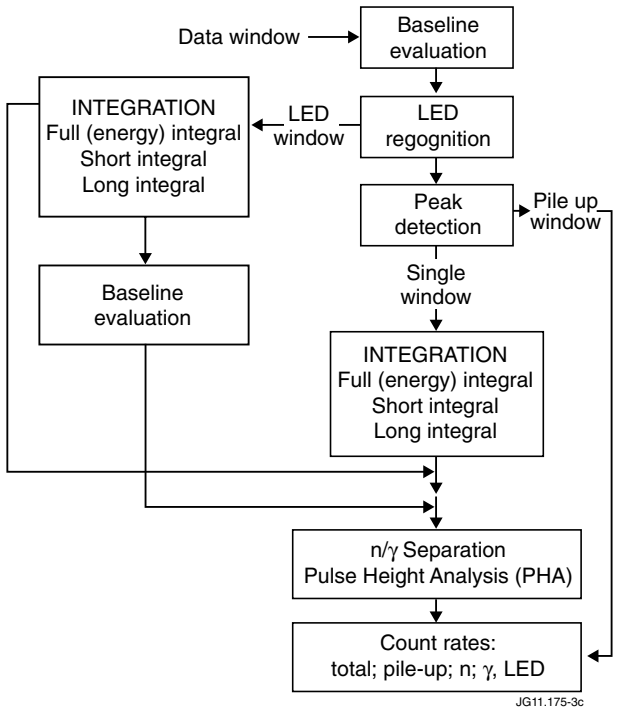

Figure 3: DPSD processing block diagram.

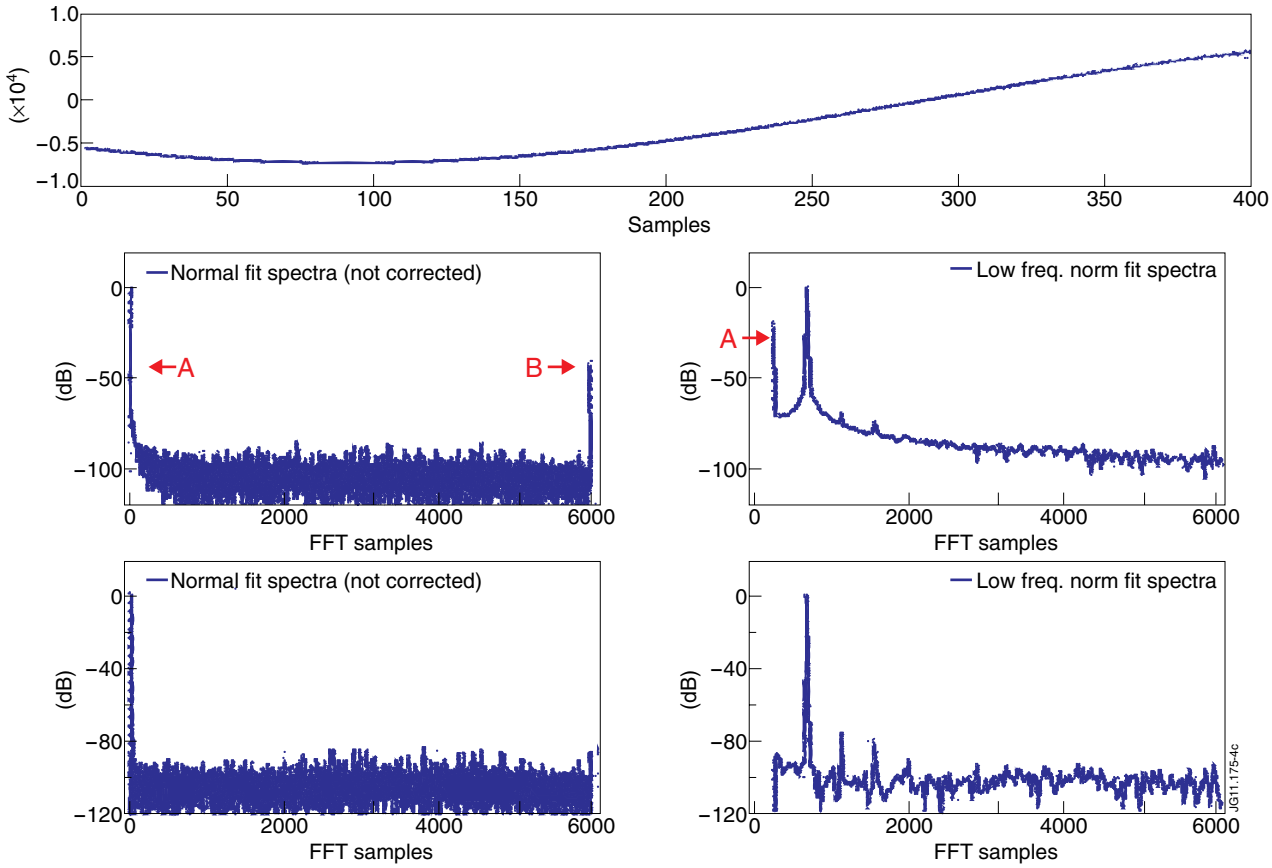

Figure 4: Calibration of the ADC acquisition channels: sinusoidal input signal (top), FFT of the uncorrected output signal (middle), FFT of the corrected output signal (bottom).

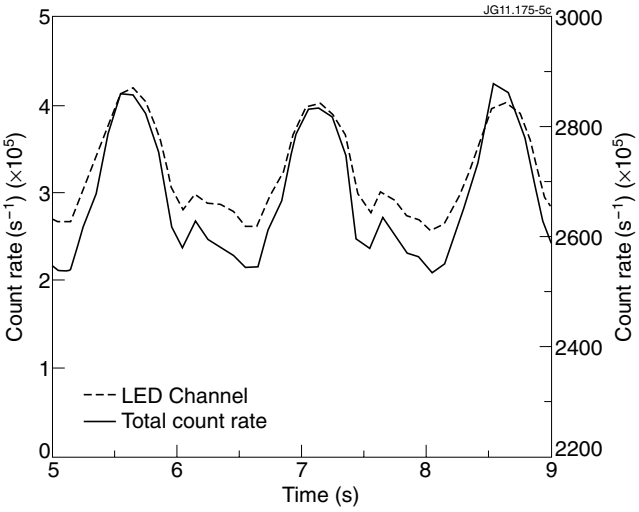

Figure 5: Total count rate (left ordinate) and position of the LED in the PHS (LED channel on the right ordinate) for a high count rate measurement performed at PTB (from [7]).

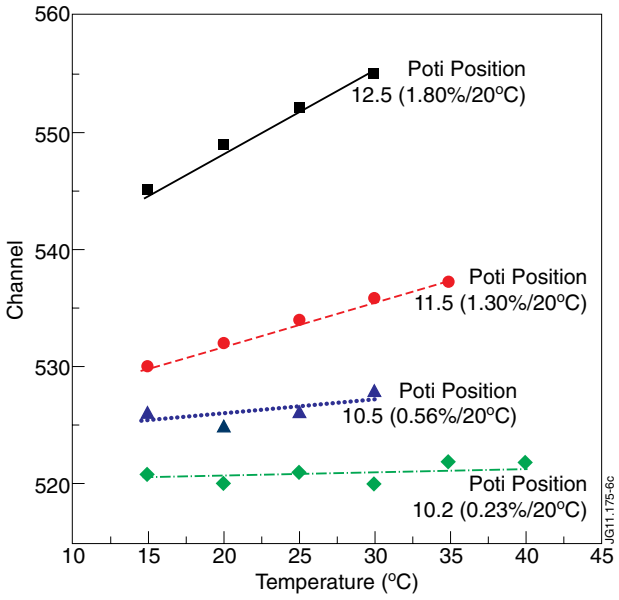

Figure 6: Difference between the PHS channel numbers of the 1274 keV and 511 keV Compton edges of ^{22}Na for different settings of the LED compensation. The setting "Pos 10,2" has been selected.

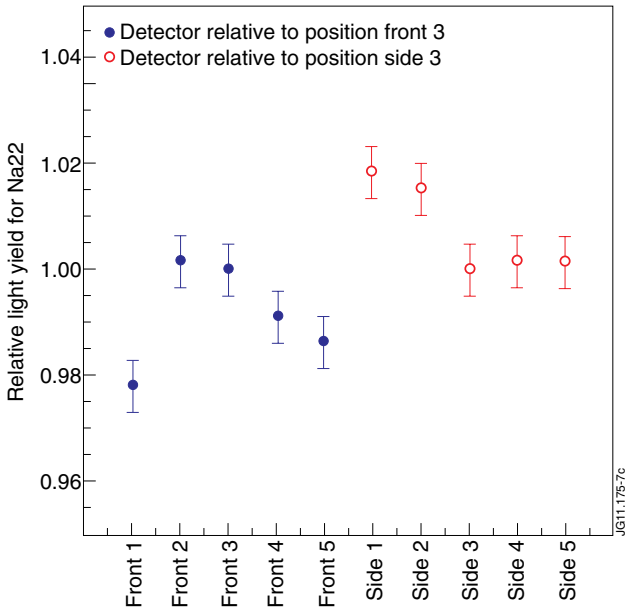

Figure 7: Response homogeneity of the PMT of the CNS (detector "Det. 31" assembly) at different radial (front) and axial (side) positions.

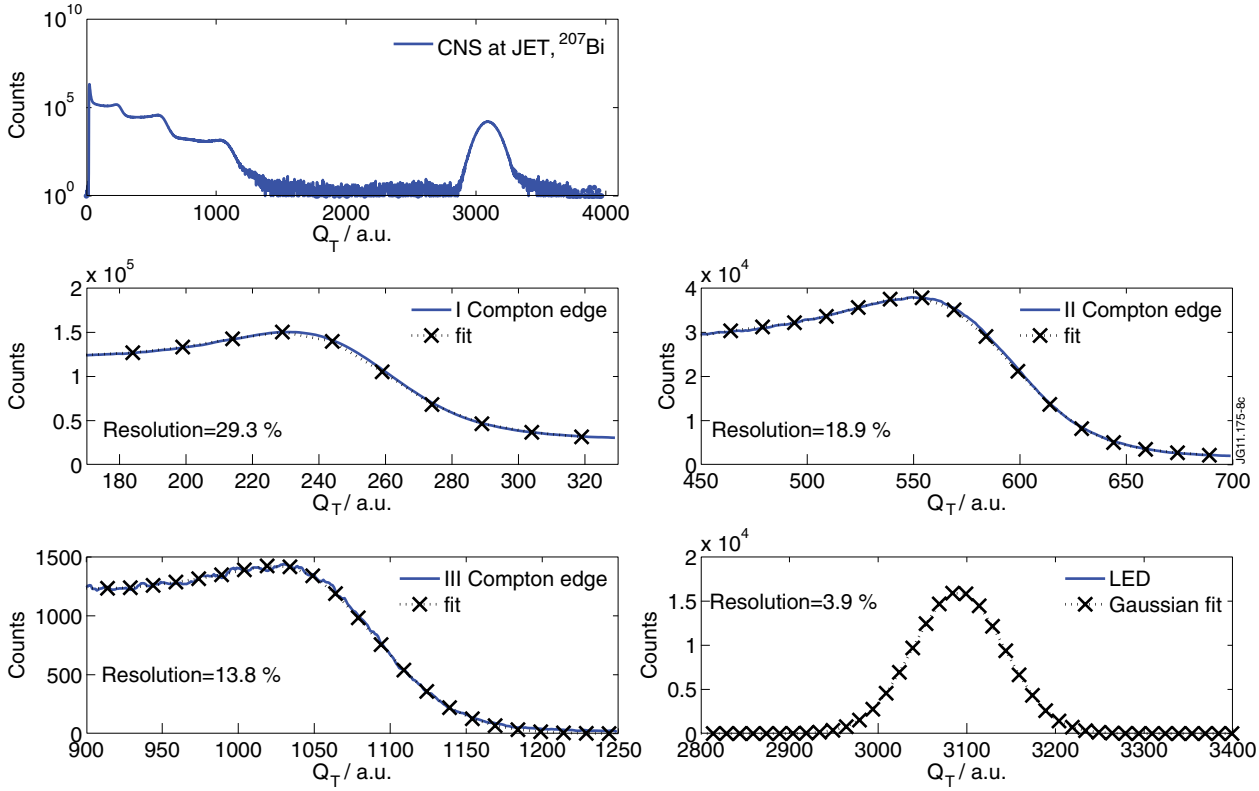

Figure 8: Pulse height resolutions measured using a ^{207}Bi calibration source.

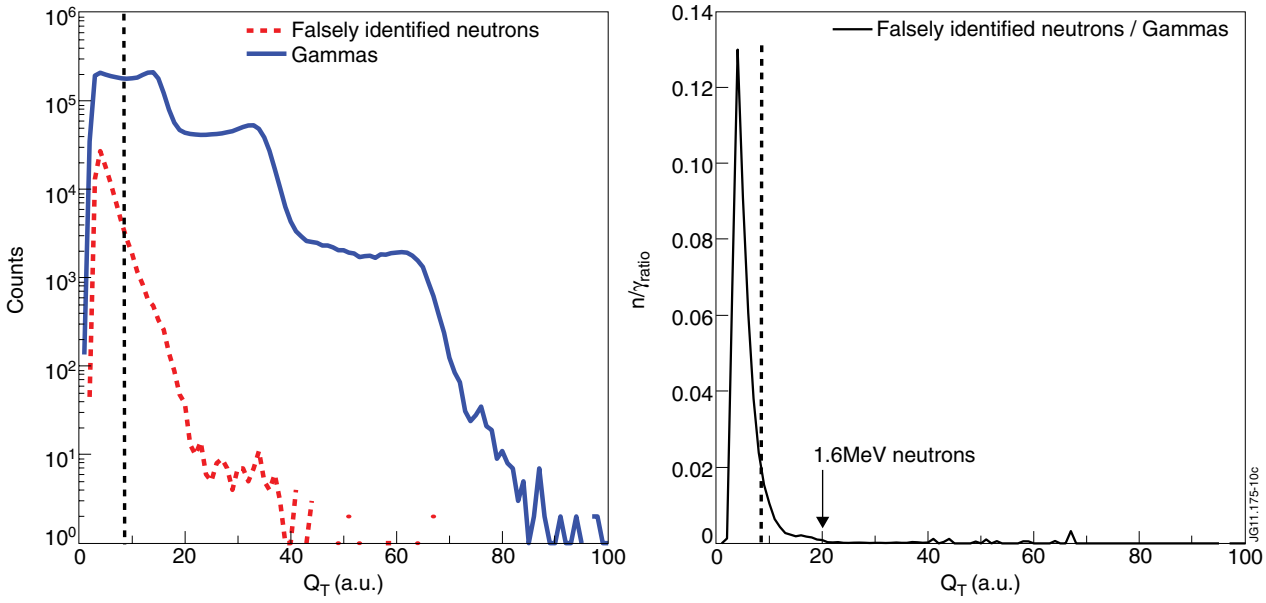

Figure 9: Results of the detector stability tests: recorded ^{207}Bi Compton edges (left) and LED peak (right) positions.

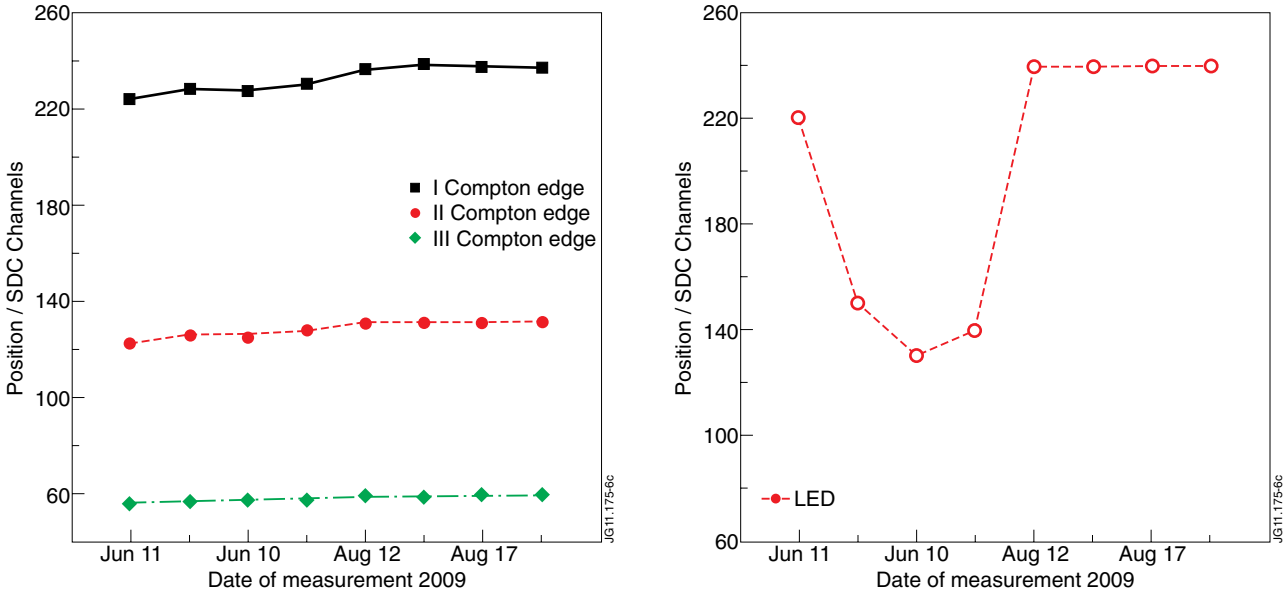

Figure 10: n and γ PHS recorded with ^{207}Bi source. The vertical dashed line indicates Q_T = 8 a.u., i.e. the threshold below which recorded pulses are discarded.

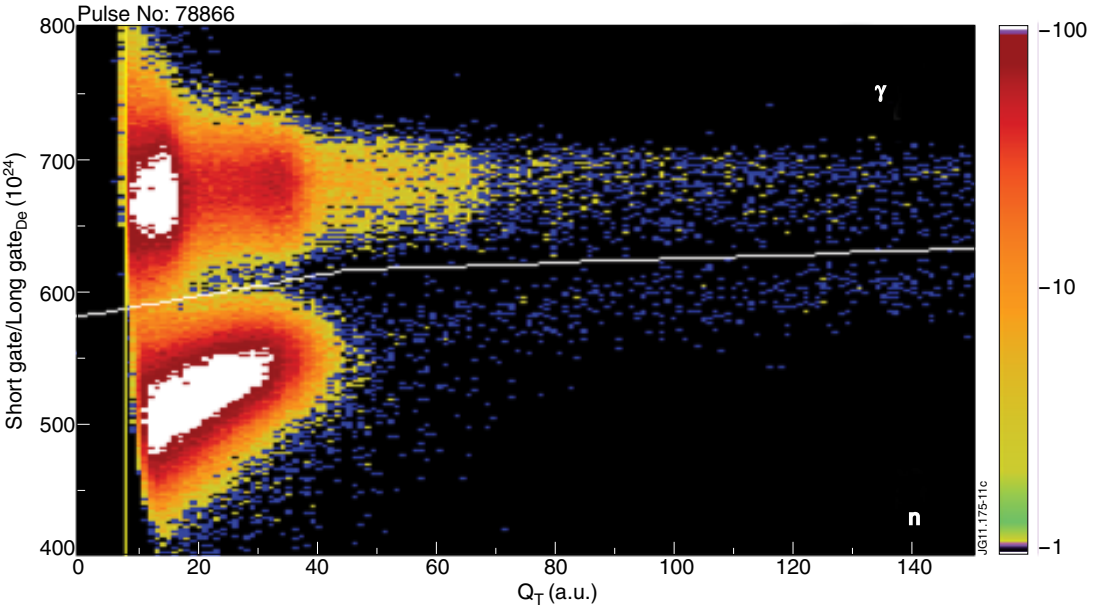

Figure 11: n/γ separation plot for JET Pulse No: 78866 for total Q_T = 8 a.u n/γ Discrimination Capability.

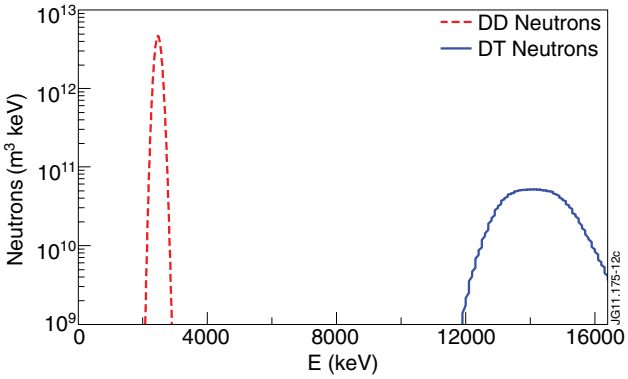

Figure 12: Calculated neutron energy spectrum produced in a 8keV D-D plasma (peak at 2.5MeV neutron energy) and by reaction of tritons with an energy of 150keV with the bulk plasma (peak at 14MeV neutron energy).

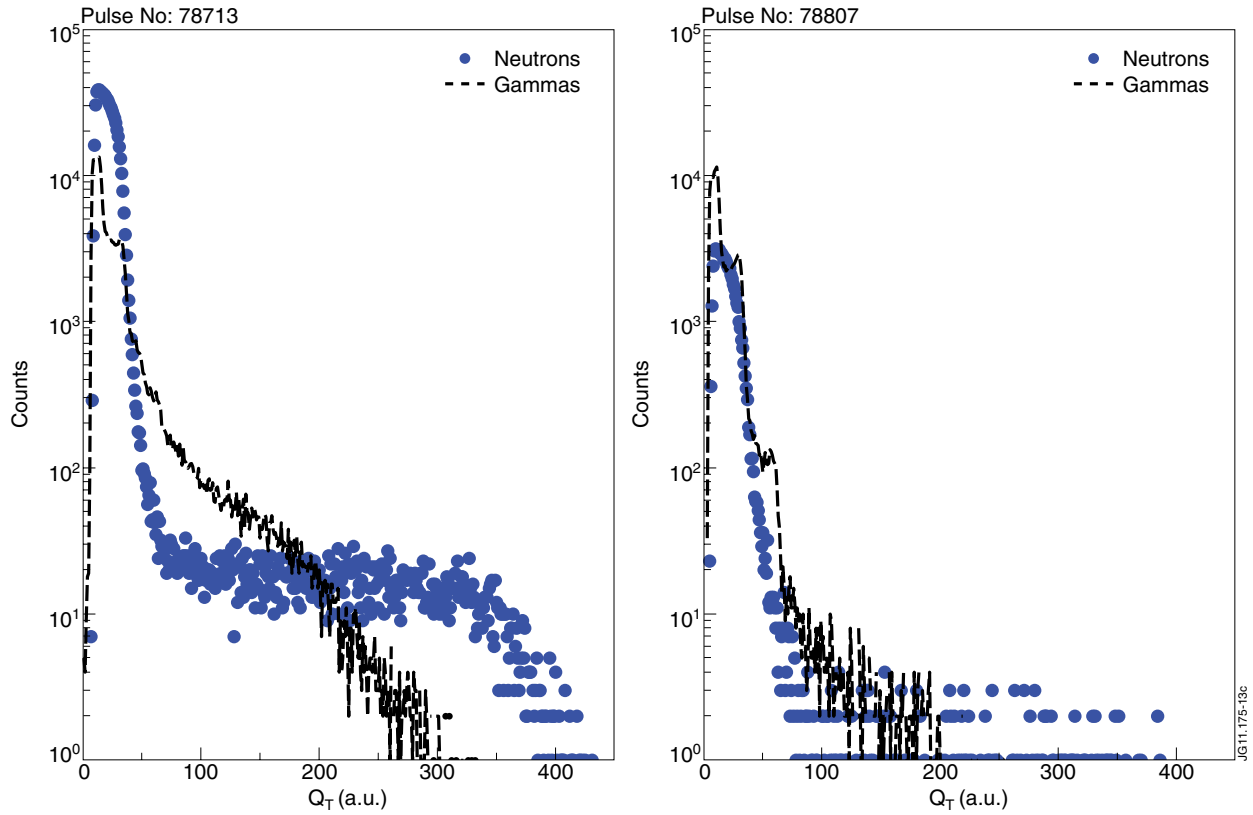

Figure 13: PHS recorded with CNS during JET pulses with high NBI power (JET Pulse No: 78713, left) and low NBI power (JET Pulse No: 78807, right).

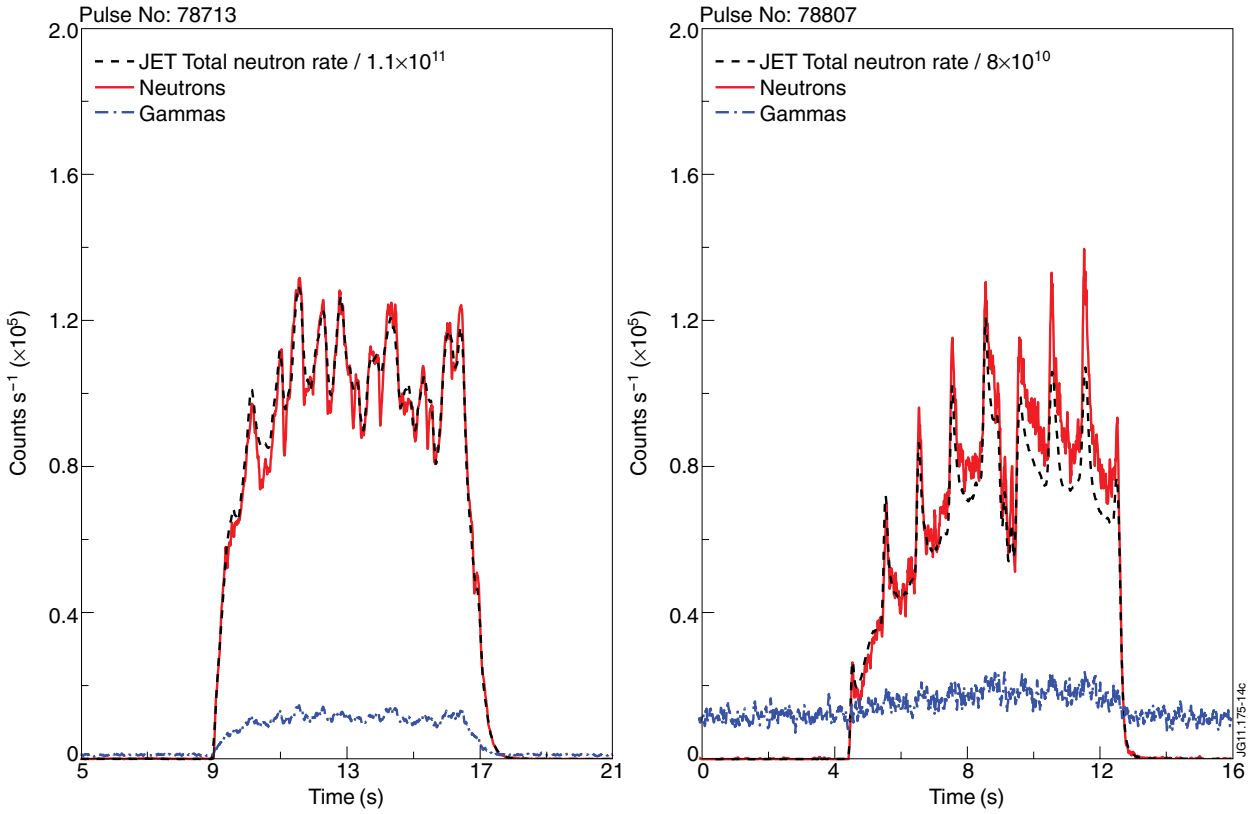

Figure 14: CNS gamma and neutrons count rates (corrected for pile-up) compared to total neutron rate measured by the JET neutron monitor (scaled as indicated in the insert) for JET pulses with high NBI power (JET Pulse No: 78713, left) and low NBI power (JET Pulse No: 78807, right).

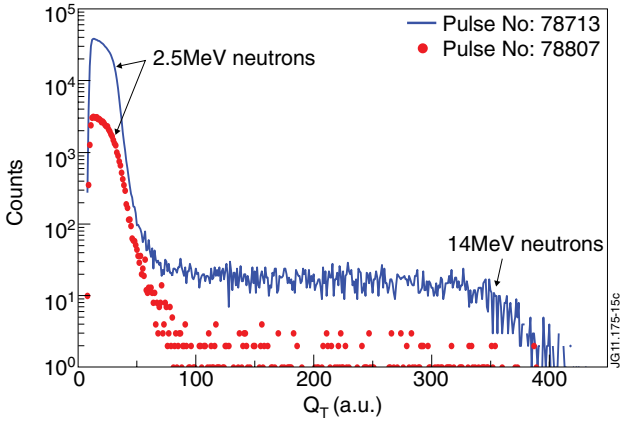

Figure 15: Comparison of the neutron PHS for high and low NBI power discharges.

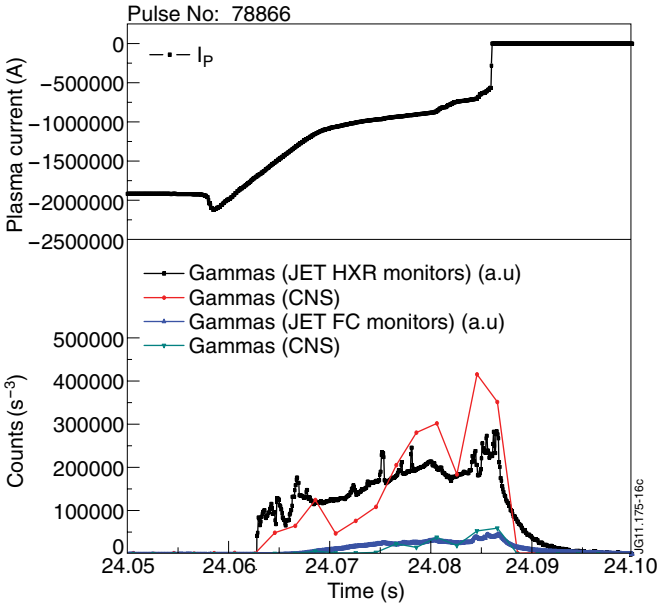

Figure 16: Plasma current (top panel) and comparison of the gamma and neutron count rates (bottom panel) measured by both the JET monitors and the CNS during a disruption event at JET.

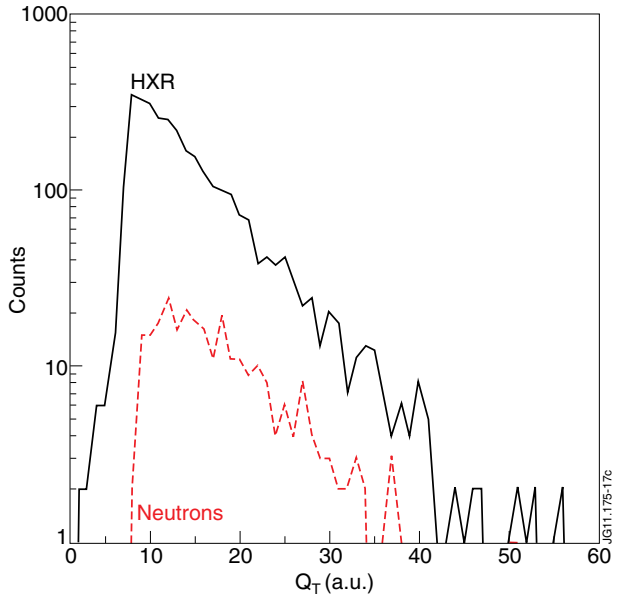

Figure 17: CNS PHS for the time interval (24.05-24.10s) of Figure 17.